Resolving the Bondi Accretion Flow Toward the Supermassive Black Hole of NGC 3115 with Chandra

Jimmy A. Irwin – University of Alabama

et al.

Citation of published version:

Wong, K., et al. (2011): Resolving the Bondi Accretion Flow Toward the Supermassive Black Hole of NGC 3115 with Chandra. *The Astrophysical Journal Letters*, 736(1). http://dx.doi.org/10.1088/2041-8205/736/1/L23

The Astrophysical Journal Letters, 736:L23 (5pp), 2011 July 20 doi:10.1088/2041-8205/736/1/L23

RESOLVING THE BONDI ACCRETION FLOW TOWARD THE SUPERMASSIVE BLACK HOLE OF NGC 3115 WITH *CHANDRA*

Ka-Wah Wong[1], Jimmy A. Irwin[1], Mihoko Yukita[1], Evan T. Million[1], William G. Mathews[2], and Joel N. Bregman[3]
[1] Department of Physics and Astronomy, University of Alabama, Box 870324, Tuscaloosa, AL 35487, USA; kwong@ua.edu
[2] UCO/Lick Observatory, Department of Astronomy and Astrophysics, University of California, Santa Cruz, CA 95064, USA
[3] Department of Astronomy, University of Michigan, 500 Church Street, Ann Arbor, MI 48109-1042, USA
Received 2011 May 31; accepted 2011 June 15; published 2011 July 1

ABSTRACT

Gas undergoing Bondi accretion onto a supermassive black hole (SMBH) becomes hotter toward smaller radii. We searched for this signature with a *Chandra* observation of the hot gas in NGC 3115, which optical observations show has a very massive SMBH. Our analysis suggests that we are resolving, for the first time, the accretion flow within the Bondi radius of an SMBH. We show that the temperature is rising toward the galaxy center as expected in all accretion models in which the black hole is gravitationally capturing the ambient gas. There is no hard central point source that could cause such an apparent rise in temperature. The data support that the Bondi radius is at about 4″–5″ (188–235 pc), suggesting an SMBH of $2 \times 10^9 M_\odot$ that is consistent with the upper end of the optical results. The density profile within the Bondi radius has a power-law index of $1.03^{+0.23}_{-0.21}$, which is consistent with gas in transition from the ambient medium and the accretion flow. The accretion rate at the Bondi radius is determined to be $\dot{M}_B = 2.2 \times 10^{-2}\ M_\odot\ \mathrm{yr}^{-1}$. Thus, the accretion luminosity with 10% radiative efficiency at the Bondi radius (10^{44} erg s^{-1}) is about six orders of magnitude higher than the upper limit of the X-ray luminosity of the nucleus.

Key words: accretion, accretion disks – black hole physics – galaxies: elliptical and lenticular, cD – galaxies: individual (NGC 3115) – galaxies: nuclei – X-rays: galaxies

Online-only material: color figures

1. INTRODUCTION

Understanding accretion onto black holes remains one of the most active areas of research in astrophysics today, both for probing black hole properties and because of their impact on larger-scale problems in galaxy and structure formation. In many nearby galaxies, the model of a central black hole gravitationally capturing ambient gas (Bondi accretion; Bondi 1952) is a vital part of our understanding of how black holes are accreting.

The key to understanding the dynamics of gas in the systems of interest lies in correctly modeling the behavior of the accreting gas once it falls within the gravitational influence of the black hole, the Bondi radius $R_B = 2GM_{\rm BH}/c_s^2$, where $M_{\rm BH}$ is the mass of the black hole and c_s is the sound speed of the gas in the vicinity of R_B. In the absence of angular momentum, the black hole is predicted to gravitationally capture the ambient interstellar medium (ISM) surrounding it at the Bondi rate $\dot{M}_B = 4\pi\lambda R_B^2 \rho c_s$, where $\lambda = 0.25$ for an adiabatic process and ρ is the density of the gas at R_B. For observed central ρ values of many nearby elliptical galaxies or Sgr A*, observed luminosities are orders of magnitude smaller than what would be predicted based on the Bondi accretion rate and assuming a standard 10% radiative efficiency (e.g., Fabian & Rees 1995). These observational results imply that the radiative efficiency of the infalling gas is exceedingly low and/or that much less material is accreted by the black hole than the Bondi formula implies.

The very weak radiation from most nearby massive black holes has prompted a significant theoretical effort aimed at explaining the very low radiative efficiencies and/or accretion rates. The central idea is that accretion proceeds via a hot radiatively inefficient accretion flow (RIAF) rather than a canonical thin accretion disk. Early RIAF models include the advection-dominated accretion flow (ADAF; Ichimaru 1977; Rees et al. 1982; Narayan & Yi 1994), the convection-dominated accretion flow (CDAF; Narayan et al. 2000; Quataert & Gruzinov 2000), and the advection-dominated inflow–outflow solution (ADIOS; Blandford & Begelman 1999).

Determining which (if any) of these scenarios describes low-L_X black hole systems is of fundamental importance to our understanding of accretion physics and black hole demography. Observational work has focused on using spatially unresolved spectral information to constrain theoretical models. While such studies have been successful in ruling out classical ADAF models in some instances (e.g., Sgr A*; Di Matteo et al. 2001; Baganoff et al. 2003), the main limitation has been the inability of even *Chandra* to resolve the accretion flow inside R_B and directly determine the density profiles of the accretion flow, as it is the shape of the density profile that most strongly distinguishes the theoretical models. While ADAFs, CDAFs, and ADIOS models all predict that the compression of gas within the accretion flow within the Bondi radius leads to a $T(R) \propto R^{-1}$ relation for the gas, the models predicted significantly different radial density profiles (Section 5).

In this Letter, we present for the first time spatially resolved temperature and density profiles within the Bondi radius of a supermassive black hole (SMBH). Dynamical modeling of the stellar kinematics of the bulge of NGC 3115 has confirmed that it harbors a (1–2) $\times 10^9 M_\odot$ black hole (Kormendy et al. 1996; Emsellem et al. 1999). At a distance of 9.7 Mpc (Tonry et al. 2001), this makes NGC 3115 the nearest $>10^9 M_\odot$ black hole. Despite its large mass, the black hole is very radio quiet, with a core 5 GHz luminosity of less than 4×10^{25} erg s^{-1} Hz^{-1} (Franceschini et al. 1998), several orders of magnitude lower than other black holes of similar mass. The black hole is also undetected in X-rays, with a *Chandra* upper limit of less than 10^{38} erg s^{-1} (Diehl & Statler 2008; K.-W. Wong et al. 2011, in preparation). The estimated Bondi accretion rate based on the

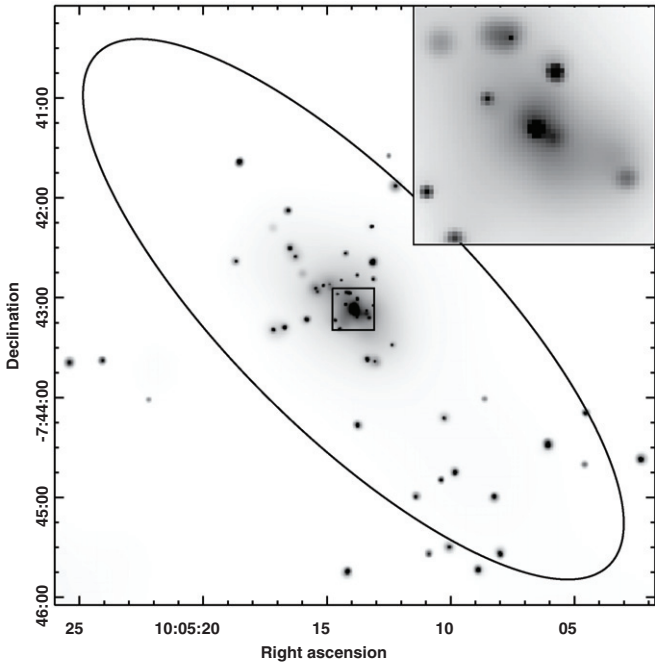

Figure 1. Smoothed 0.3–6.0 keV *Chandra* image of NGC 3115 with D_{25} (de Vaucouleurs et al. 1991) optical contour. The inset is the 2.0–6.0 keV image of the central $25'' \times 25''$ region. There is not a point source at the center, but a plateau in the diffuse X-ray surface brightness.

previous observed density of ≈ 0.1 cm^{-3} (David et al. 2006) in the central part of the galaxy is $\sim 0.1\, M_\odot$ yr^{-1}, implying an expected luminosity $\sim 10^{45}$ erg s^{-1} if accretion occurred with 10% efficiency. The lack of radio power argues that it is unlikely that jets are interacting strongly with the gas inside R_B.

2. X-RAY OBSERVATIONS AND SPECTRAL ANALYSIS

NGC 3115 (Figure 1) was observed with *Chandra* on 2001 June 14, 2010 January 27, and 2010 January 29 for 37, 41, and 77 ks, respectively. All the data were reprocessed using the *Chandra* Interactive Analysis of Observations (CIAO) software version 4.3 and the *Chandra* Calibration Database (CALDB) version 4.4.1. We used a local background that is extracted from the $70''$–$90''$ annulus centered at the X-ray peak. The background region is far enough from the center so that the source-removed surface brightness of the X-ray emission is basically flat beyond $70''$. The background only contributes less than about 1% of the emission (0.5–6.0 keV) within the Bondi radius ($\lesssim 5''$) and less than about 7% for the ambient region beyond the Bondi flow ($4''$–$10''$). Errors are given at 1σ level unless otherwise specified.

We extracted spectra in annuli centered at the central peak of the extended X-ray emission. This peak was detected as a source by CIAO *wavdetect*. However, further analysis shows that a modeled circular Gaussian width of this peak emission is twice extended as that of a nearby bright point source and that the central source is static (varied less than 2σ) within and between the observations. Thus, it is dominated by a concentration of hot gas and unresolved binaries rather than a single compact accreting object. We included this peak emission but excluded all the other sources detected by *wavdetect* during the analysis.

The unresolved X-ray emission is mainly contributed by unresolved low-mass X-ray binaries (LMXBs), cataclysmic variables and coronally active binaries (CV/ABs), and the diffuse hot gas component that we are interested in. The very soft emission from the gas and the very hard emission from the unresolved LMXBs are easy to separate spectrally. No appreciable emission is expected from the gas above 2 keV, so we can use the 2–6 keV emission as a lever arm for estimating the amount of unresolved LMXB flux in the 0.5–2.0 keV band and subtract it accordingly if we assume an appropriate spectral model for the LMXBs. Irwin et al. (2003) have shown that the summed spectra of resolved low-L_X ($<10^{37}$ erg s^{-1}) LMXBs in the bulge of M31 are very similar to more luminous LMXBs. Hence, it is valid to assume that the unresolved LMXB emission can be spectrally modeled as the brighter resolved sources. We found that the fainter, softer source like those that make up the Galactic Ridge emission (CV/AB) contributes similarly to the soft flux of the gas based on L_X–L_K scaling relations within $4''$ for this component, where L_K is the Two Micron All Sky Survey (2MASS) K-band luminosity. Hence, including this component is essential in the analysis.

For the LMXB component, we take $\Gamma_{\rm LMXB} = 1.61^{+0.02}_{-0.02}$ measured from the combined spectrum of all the resolved point sources within D_{25} of NGC 3115. For the CV/AB component, we fitted the unresolved X-ray emission of M32, which is believed to be truly gas free (Revnivtsev et al. 2007; Boroson et al. 2011), using an absorbed thermal + power-law model. The best-fit temperature is $T_{\rm CV/AB} = 0.59^{+0.05}_{-0.13}$ keV and the power-law index is $\Gamma_{\rm CV/AB} = 1.93^{+0.09}_{-0.09}$, which are consistent with the values measured by Revnivtsev et al. (2008). The CV/AB normalizations of each annulus are determined by the L_X–L_K scaling relation derived from M32.

We used the X-ray Spectral Fitting Package[4] (XSPEC) for spectral analysis. The 2001 and 2010 spectra of each annulus in the 0.5–6.0 keV energy range were fitted jointly to the three-component absorbed model (PHABS in XSPEC)—a thermal model (APEC in XSPEC) for the gas, a power-law (POWERLAW in XSPEC) for the unresolved LMXBs, and a combination of thermal + power-law (APEC + POWERLAW) model for the CV/ABs. The absorption is fixed at the Galactic value of $N_{\rm H} = 4.32 \times 10^{20}$ cm^{-2} (Dickey & Lockman 1990). We fit the temperature of the thermal gas component. The normalizations of the thermal gas and the LMXB components are allowed to vary and untied. Since the abundance cannot be constrained from the spectra, we fixed it to solar value. Using 0.2 solar only increases the best-fit temperature by $\lesssim 10\%$ and increases the gas normalizations by a factor of four. The derived density only increases by a factor of two and all our conclusions remain the same. All the other parameters are fixed as described above. The spectra were fitted using the c-statistic. Varying $\Gamma_{\rm LMXB}$ or $\Gamma_{\rm CV/AB}$ by their 1σ uncertainties or varying the CV/AB normalizations by $\pm 20\%$ (that is larger than their 1σ uncertainties) only changes the best-fit gas temperature or the gas normalizations by $<9\%$.

3. TEMPERATURE PROFILE

The projected temperature profile is shown in the upper panel of Figure 2. Although the error bars are quite large, it can be seen that the trend is rising toward the center as expected in a Bondi flow. We have also constructed a physical model with a temperature profile expected in a Bondi flow (i.e., $T \propto R^{-1}$) and a density profile taken from our best-fit model ($\rho(R) \propto R^{-1}$; see Section 4 below). The simulated projected temperature profile is consistent with our measured profile. In particular, the simulated projected temperature within the $2''$ region is biased

[4] http://heasarc.nasa.gov/xanadu/xspec/

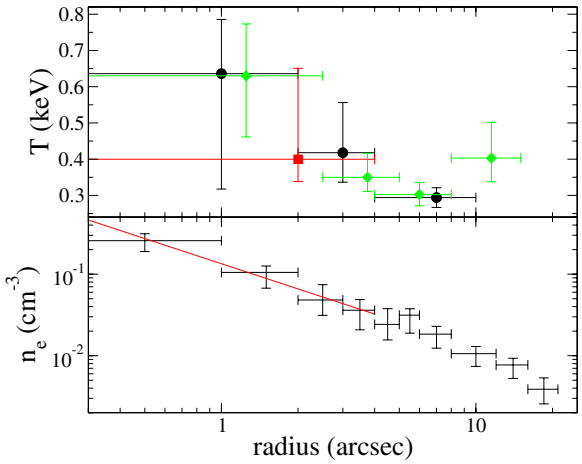

Figure 2. Upper panel: projected temperature profile of the hot gas component. Different colors are with different binnings. Lower panel: deprojected density profile. The best-fit power-law model within 4″ is shown in solid line.

(A color version of this figure is available in the online journal.)

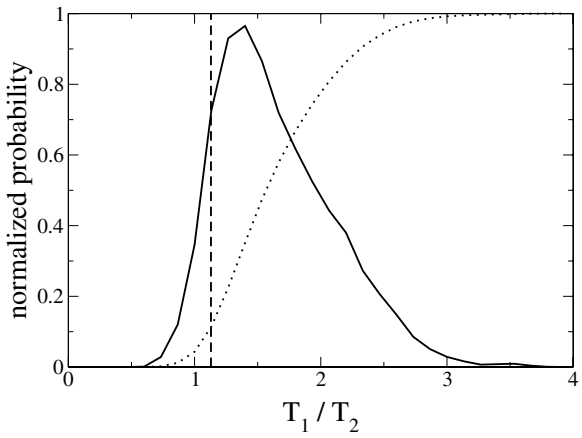

Figure 3. Normalized probability (solid line) and the cumulative probability (dotted line) of the simulated temperature ratios between the 2″–4″ (T_1) and the 4″–10″ (T_2) annuli. The vertical line cuts the cumulative probability at 10%.

low with respect to the deprojected (physical) temperature and is consistent with our measured low value. Thus, the bias in the central temperature may be explained by the projection of the cooler gas from the outer region.

For a measured ISM temperature of 0.3 keV in the outer most bin, this corresponds to $R_B = 112$–224 pc (2.″4–4.″8) depending on the adopted black hole mass estimate ($(1–2) \times 10^9\ M_\odot$). Careful selection of the boundary radius suggests that the onset in the increase in temperature begins at 4″–5″, rather than at 2″. To confirm this, we have performed a Markov chain Monte Carlo (MCMC) simulation to address the significance of the rise in temperature just within a radius of 4″. The distribution (normalized probability) and the cumulative probability of the simulated temperature ratios between the 2″–4″ and the 4″–10″ annuli are plotted in Figure 3. The MCMC test suggests that the temperature ratio is larger than 1.13 at the 90% confidence level. Assuming that the temperature beyond R_B is constant and $T \propto R^{-1}$ inside R_B,[5] the expected temperature ratio at 3″ and at R_B (4″) is 1.33, which is consistent with the peak ratio of 1.4 in the MCMC simulation.

[5] Note that the temperature profile can be flatter in the transition region between the ambient ISM and the central accretion flow near ∼0.1–1 R_B (Quataert 2002).

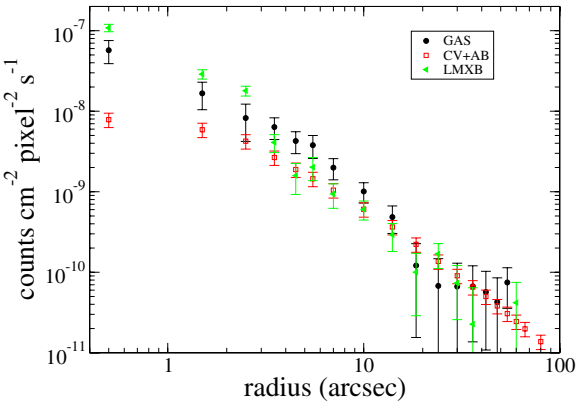

Figure 4. Surface brightness profile for the hot gas (black circles), CV/AB (red open squares), and LMXB (green triangles) components in the 0.5–1.0 keV band.

(A color version of this figure is available in the online journal.)

The harder spectrum within 4″ is not the spurious result of any hard central point source. We obtained the same overall result even when we excised the inner 1″. The effect of unresolved X-ray binaries has been properly accounted for by quantifying the unresolved emission in the 2.0–6.0 keV band and extrapolating to lower energies. The effect of a large number of softer accreting white dwarfs, stellar coronae, etc., has also been taken into account in our analysis. Such an increase in the temperature is exactly what is expected in all models in which the black hole is gravitationally capturing the ambient gas (see, e.g., Quataert & Narayan 1999; Quataert & Gruzinov 2000). In fact, a similar spike in ISM temperature was found at the center of NGC 4649 and was interpreted as confirmation of a $>10^9\ M_\odot$ black hole (Humphrey et al. 2008), although in this galaxy R_B is unresolved by *Chandra*. Finally, the lack of detectable radio emission from the core of NGC 3115 argues against heating of the gas from jets.

4. SURFACE BRIGHTNESS AND DENSITY PROFILES

We have calculated the surface brightness profiles for the thermal gas, CV/AB, and LMXB components. The CV/AB profile was calculated using the same L_X–L_K scaling relations mentioned above. The LMXB profile was calculated by assuming that the emission above 2 keV is contributed by the LMXBs only, and its contribution to the soft emission was calculated by the assumed spectral model above. The gas profile in the soft band was calculated by subtracting the CV/AB and LMXB contributions. Figure 4 shows the surface brightness profiles for the three components in the 0.5–1.0 keV energy band. The upper limit is chosen to maximize the contribution from the gas component with respect to the other two components. Note that the gas component is clearly detected within ∼15″ and is rising more steeply compared with the stellar (CV/AB) component toward the center.

With the surface brightness profile for the hot gas component, the electron density profile can be deprojected. We converted the count rate in each annulus into flux using the XSPEC APEC model with a temperature of 0.45 keV and solar abundance. The temperature was taken as the mid value of the best-fit temperature of the central 0″–2″ bin and the ambient temperature. Since the emissivity mainly depends on density, the precise value of temperature is not important at our level of accuracy. We have tested the density profiles derived using different

temperatures between 0.3–0.6 keV. All the derived density profiles are consistent within the error bars. The flux was then deprojected into emissivity, ϵ, at each radius using a method described in Wong et al. (2008) and also described in Kriss et al. (1983). This technique calculates the emission measures of each spherical shell starting from the outer most annulus toward the center, and the emission measure of each subsequent shell is calculated by subtracting the projected emission from the outer shells. The electron density can then be converted from the emissivity by the relation $\epsilon = n_e^2\Lambda$, where the emissivity function Λ depends on the temperature and the abundance. The emissivity function is taken from the same APEC model.

The deprojected electron density profile is shown in the lower panel of Figure 2. The errors were estimated by running 10^6 Monte Carlo simulations. Fitting the density profile within $4''$ to a power law gives $\rho \propto R^{-[1.03^{+0.23}_{-0.21}]}$. This is consistent with the power-law index of $1.14^{+0.29}_{-0.28}$ in the $4''$–$25''$ region.

5. DISCUSSION

Accretion models predict that gas within the Bondi radius flows toward the SMBH. The increases in the temperature and density of thermal gas toward the center are direct evidence that the gas is being gravitationally captured by the SMBH. Resolving the temperature and density profiles within the Bondi radius can provide tight constraints to accretion models.

Our 150 ks *Chandra* observation of NGC 3115 supports that there is a rise in temperature inside R_B compared to the galaxy's ISM temperature outside R_B, exactly as expected from accretion models. We have shown that the onset in the increase in temperature begins at $\approx 4''$–$5''$ rather than at $2''$. This supports that the mass of the SMBH is at the upper end of the (1–2) $\times\ 10^9 M_\odot$ range (Kormendy et al. 1996; Emsellem et al. 1999).

In previous studies where the Bondi accretion flow could not be spatially resolved, the overall spectrum has to be modeled to constrain accretion model. With the spatially resolved spectra we have measured, we can draw definite conclusion for the first time on the dynamical properties within the Bondi radius. In these regions ($R > 100\,R_S$, where $R_S = 2GM_{\rm BH}/c^2$ is the Schwarzschild radius), the electron temperature is fairly well determined since the gas is essentially virial and one temperature (Quataert & Narayan 1999). Therefore, observations of the bremsstrahlung emission in X-ray give direct information on the density of the outer regions of the Bondi flow and thereby the accretion rate on the outside ($\dot{M}(R > 100\,R_S)$).

Because the uncertainties in our measurements are still large, we do not attempt to compare the observational results to state-of-art theoretical models. Instead, we focus on the simplest classical models. In the early analytic models (ADAFs; Ichimaru 1977; Rees et al. 1982; Narayan & Yi 1994) it was argued that the radiative efficiency is low because the accretion flow is a hot two-temperature plasma in which most of the energy is carried into the black hole by the ions. If the electrons—which produce the radiation we observe—receive very little of the energy in the system, the radiative efficiency will be much lower than the standard value of $\sim$10%. In ADAF models, the accretion rate is argued to be similar to the Bondi rate and the dynamics of the inflowing gas is similar to that of spherical Bondi accretion, even though the inflow has angular momentum. Contrary to ADAF and Bondi predictions, more recent analytic models suggest that when the radiative efficiency is low, very little of the mass available at large radii actually accretes onto the black hole, with most of it being blown away at all radii in an outflow (ADIOS; Blandford & Begelman 1999) or continuously circulating in convective eddies (CDAF; Narayan et al. 2000; Quataert & Gruzinov 2000). Accretion rates $\ll \dot{M}_B$ are strongly supported by global numerical simulations of thick disk accretion (e.g., Igumenshchev & Abramowicz 1999; Stone et al. 1999; Hawley & Balbus 2002; Igumenshchev et al. 2003).

Here, we assume the self-similar structure of the accretion models extends from the vicinity of the SMBH out to the Bondi radius (see, e.g., Abramowicz et al. 2002). In the classic Bondi/ADAF models, $\rho(R) \propto R^{-3/2}$, while in CDAFs the redistribution of gas via convection predicts a much flatter density profile, $\rho(R) \propto R^{-1/2}$. The ADIOS models allow the accretion rate to vary with radius and the density profile is modified as $\rho(R) \propto R^{-3/2+p}$, where $p \approx 0$–1 characterize the density and accretion rate suppression. In our 150 ks observation, we have constrained $p = 0.47^{+0.21}_{-0.23}$ from the density profile, which is consistent with the value of $p \approx 0.6$ measured from the spatially unresolved spectrum of Sgr A* by Baganoff et al. (2003), although they cannot put constraints from their data. Taken at face value, we have barely ruled out the classical Bondi/ADAF model and the classical CDAF model at about 2σ, provided that the density profile has a single power-law index within R_B.

However, theoretical models also suggest that the regions we have resolved are still in transition from the ambient ISM to the accretion flow (Quataert 2002) and the slope in these regions can be different from the asymptotic behavior. The measured density slope within R_B is consistent with that beyond. Thus, the ADAF/CDAF models might not be ruled out. More theoretical work is needed to interpret the data. Nevertheless, the data suggest that the transition does not finish until at least $\sim$0.2 R_B for either the classical Bondi/ADAF or the CDAF models. The density profile around $\sim$0.1–1 R_B does provide some direct constraints to theoretical models, e.g., thermal conduction can change the power-law index of the density by about 0.5 around those regions (Johnson & Quataert 2007).

We determined that the Bondi accretion rate of NGC 3115 is $\dot{M}_B = 2.2 \times 10^{-2}\,M_\odot\ {\rm yr}^{-1}$. Assuming a 10% radiative efficiency, the accretion luminosity at R_B (10^{44} erg s^{-1}) is about six orders of magnitude higher than the upper limit of the X-ray luminosity of the nucleus. Such a discrepancy can be explained if the accretion rate is lower than the classical Bondi rate. For example, the accretion rate for the ADIOS or CDAF models is suppressed and scales with radius as $\dot{M}_{\rm acc} \sim \alpha \dot{M}_B (R/R_B)^p$, where α is the dimensionless viscosity parameter in the standard thin disk model (Shakura & Sunyaev 1973; Baganoff et al. 2003). Using a typical value of $\alpha \sim 0.1$ to calculate $\dot{M}_{\rm acc}$ at R_S, p should be close to 1 to explain the discrepancy. It is also quite possible that the gas has non-negligible angular momentum that should be more important at smaller radii. This can reduce the accretion rate near the event horizon (e.g., Proga & Begelman 2003). Alternatively, the radiation efficiency can be lower than the canonical value of 0.1 (e.g., Ho 2008).

Currently, the uncertainties are limited by the statistics of our data. A deep *Chandra* observation will improve the statistics to provide useful constraints to accretion models.

We thank Eliot Quataert and the referee for helpful discussions. This work was supported by NASA LTSA grant NNG05GE48G and *Chandra* grant GO0-11101A.

REFERENCES

Abramowicz, M. A., Igumenshchev, I. V., Quataert, E., & Narayan, R. 2002, ApJ, 565, 1101
Baganoff, F. K., et al. 2003, ApJ, 591, 891
Blandford, R. D., & Begelman, M. C. 1999, MNRAS, 303, L1
Bondi, H. 1952, MNRAS, 112, 195
Boroson, B., Kim, D.-W., & Fabbiano, G. 2011, ApJ, 729, 12
David, L. P., Jones, C., Forman, W., Vargas, I. M., & Nulsen, P. 2006, ApJ, 653, 207
de Vaucouleurs, G., de Vaucouleurs, A., Corwin, H. G., Jr., Buta, R. J., Paturel, G., & Fouque, P. 1991, Third Reference Catalogue of Bright Galaxies (Berlin: Springer)
Dickey, J. M., & Lockman, F. J. 1990, ARA&A, 28, 215
Diehl, S., & Statler, T. S. 2008, ApJ, 680, 897
Di Matteo, T., Johnstone, R. M., Allen, S. W., & Fabian, A. C. 2001, ApJ, 550, L19
Emsellem, E., Dejonghe, H., & Bacon, R. 1999, MNRAS, 303, 495
Fabian, A. C., & Rees, M. J. 1995, MNRAS, 277, L55
Franceschini, A., Vercellone, S., & Fabian, A. 1998, MNRAS, 297, 817
Hawley, J. F., & Balbus, S. A. 2002, ApJ, 573, 738
Ho, L. C. 2008, ARA&A, 46, 475
Humphrey, P. J., Buote, D. A., Brighenti, F., Gebhardt, K., & Mathews, W. G. 2008, ApJ, 683, 161
Ichimaru, S. 1977, ApJ, 214, 840
Igumenshchev, I. V., & Abramowicz, M. A. 1999, MNRAS, 303, 309
Igumenshchev, I. V., Narayan, R., & Abramowicz, M. A. 2003, ApJ, 592, 1042
Irwin, J. A., Athey, A. E., & Bregman, J. N. 2003, ApJ, 587, 356
Johnson, B. M., & Quataert, E. 2007, ApJ, 660, 1273
Kormendy, J., et al. 1996, ApJ, 459, L57
Kriss, G. A., Cioffi, D. F., & Canizares, C. R. 1983, ApJ, 272, 439
Narayan, R., Igumenshchev, I. V., & Abramowicz, M. A. 2000, ApJ, 539, 798
Narayan, R., & Yi, I. 1994, ApJ, 428, L13
Proga, D., & Begelman, M. C. 2003, ApJ, 592, 767
Quataert, E. 2002, ApJ, 575, 855
Quataert, E., & Gruzinov, A. 2000, ApJ, 539, 809
Quataert, E., & Narayan, R. 1999, ApJ, 520, 298
Rees, M. J., Begelman, M. C., Blandford, R. D., & Phinney, E. S. 1982, Nature, 295, 17
Revnivtsev, M., Churazov, E., Sazonov, S., Forman, W., & Jones, C. 2007, A&A, 473, 783
Revnivtsev, M., Churazov, E., Sazonov, S., Forman, W., & Jones, C. 2008, A&A, 490, 37
Shakura, N. I., & Sunyaev, R. A. 1973, A&A, 24, 337
Stone, J. M., Pringle, J. E., & Begelman, M. 1999, MNRAS, 310, 1002
Tonry, J. L., Dressler, A., Blakeslee, J. P., Ajhar, E. A., Fletcher, A. B., Luppino, G. A., Metzger, M. R., & Moore, C. B. 2001, ApJ, 546, 681
Wong, K.-W., Sarazin, C. L., Blanton, E. L., & Reiprich, T. H. 2008, ApJ, 682, 155